Energy spectra of steady two-dimensional turbulent flows

Norbert Schorghofer
Department of Physics, Chinese University of Hong Kong, Shatin, Hong Kong
(Received 8 October 1999)

The power spectrum is measured in direct numerical simulations of the two-dimensional Navier-Stokes equation and other two-dimensional flows with white-in-time forcing at large scales. For the Navier-Stokes equation the energy spectrum in the inertial range approaches k^{-3} with increasing Reynolds number, with possible logarithmic corrections. A family of two-dimensional flows, including the surface quasigeostrophic equation, allows us to vary the locality of the ''enstrophy'' transfer, where enstrophy is the mean square of the convected quantity. Dimensional analysis based on the enstrophy dissipation correctly predicts the energy spectrum, whenever the enstrophy transfer can be assumed to be spectrally local. Otherwise, the enstrophy spectrum is steeper than would be expected on the basis of local transfer. In this case the data suggest a k^{-1} passive scalar spectrum.

PACS number(s): 47.27.Gs, 47.27.Ak, 92.90.+x

I. INTRODUCTION

More than 30 years ago the energy spectrum of two-dimensional turbulence was theoretically predicted. Yet the evidence for this spectrum has remained weak in some cases. Classical theory [1–3] predicts the energy spectrum based on a ''cascade'' of either energy or enstrophy. Once the relevant physical quantities have been identified, simple dimensional analysis leads to the power spectrum as a function of wave number k. However, the spectra measured in many numerical simulations decay substantially faster with k than predicted [4].

The range of wave numbers larger than the inverse system size and up to the dissipative damping is called ''inertial range.'' In this paper we assume power laws for the inertial range as a ''working hypothesis,'' since possible deviations from a power behavior cannot be determined from numerical data with confidence.

A general review of two-dimensional turbulence and the slope of the energy spectrum can be found in Refs. [5,6]. Following, we summarize recent results on the inertial-range spectrum.

For *decaying* two-dimensional turbulence a spectrum proportional to k^{-3} has by now been clearly observed for the late stage of the evolution, see, e.g., Refs. [7,8]. With forcing at *small* scales evidence for the predicted $k^{-5/3}$ is less clear. In a detailed analysis, Borue [9] found k^{-3} resulting from strong vortices and a $k^{-5/3}$ background field. Least reported is two-dimensional turbulence forced at *large* scales. High-resolution simulations by Gotoh *et al.* [10–12] have demonstrated relatively flat spectra, which become less and less steep as the Reynolds number increases, and indeed appear to approach k^{-3}. Similar observations have been made by Borue [13]. Experimentally, two-dimensional Navier-Stokes turbulence is difficult to realize, although there has been much progress recently (see Ref. [14]).

The k^{-3} law follows from dimensional analysis [2,3]. Closure theory gives a logarithmic correction $k^{-3}\log(k/k_I)^{-1/3}$. Dimensional analysis requires us to choose the relevant physical quantities and predicts different exponents depending on this choice. Saffman proposed a spectrum of k^{-4} based on vorticity discontinuities [15]: an otherwise smooth function punctured by jump discontinuities has Fourier coefficients $\sim k^{-1}$, which corresponds to a k^{-4} energy spectrum. An idea [16,17] to bridge the discrepancy between k^{-3} and k^{-4} was to consider accumulations of discontinuities through spiral vortices, and suggests $k^{-11/3}$ (over a fixed range of k only). Others [18,19] proposed that spectra steeper than k^{-3} arise from strong vortices that are distributed over different length-scales according to a power law. Which is the correct theory?

In Sec. II we study the inertial range energy spectrum of the two-dimensional Navier-Stokes equation. In Sec. III we turn to a more general family of flows, which allows us to test the applicability of the various theories. Conclusions are found in the last section.

II. NAVIER-STOKES FORCED AT LARGE SCALES

The two-dimensional Navier-Stokes equation takes the form of an advection-diffusion equation for the vorticity $\omega = \vec{\nabla}\times\vec{v}$,

$$\frac{\partial\omega}{\partial t} + \vec{v}\cdot\vec{\nabla}\omega = D\nabla^2\omega + f. \tag{1}$$

In two dimensions, vorticity is a scalar quantity. The forcing f supplies the energy dissipated via a dissipation constant D. Half of the square of the vorticity is called ''enstrophy.''

A. Design of simulations

The flow is simulated in a doubly periodic box of size $2\pi\times 2\pi$. Forcing acts on large scales $4\leqslant|k|<6$, with constant amplitude but random phases renewed at each time step. The Fourier method is used for spatial derivatives and fourth-order Runge-Kutta is employed for time integration. The constant time step $\Delta t\approx 0.5\Delta x/\max(|v_x|+|v_y|)$. This formula is appropriate from linear stability analysis of the advection equation and the coefficient in front is empirically determined.

In two-dimensional flows, vortices merge and grow ever larger. These vortices must be destroyed in order to reach a

TABLE I. List of runs and their parameters. N = number of grid points on each side. The total time T over which measurements are taken starts after a prior period of relaxation to equilibrium. Averages $\langle\ \rangle$ are over all space and a number of instances of time. The enstrophy dissipation $\varepsilon = D\langle(\nabla\theta)^2\rangle$.

α	N	T	D	$\langle\vec{v}^2\rangle$	$\langle\theta^2\rangle$	ε
1	256	67	1×10^{-3}	0.38	0.38	5.3×10^{-3}
1	512	134	5×10^{-4}	0.48	0.48	5.0×10^{-3}
1	1024	59	2×10^{-4}	0.61	0.61	4.9×10^{-3}
1	2048	3	9×10^{-5}	0.63	0.63	4.1×10^{-3}
2	256	4021	5×10^{-4}	0.044	0.46	5.6×10^{-3}
2	512	247	2×10^{-4}	0.056	0.58	5.6×10^{-3}
2	1024	300	6×10^{-5}	0.073	0.91	5.2×10^{-3}
2	2048	8	2×10^{-5}	0.085	1.2	5.3×10^{-3}
3	256	167	2×10^{-4}	5.4×10^{-3}	0.84	5.6×10^{-3}
3	512	804	6×10^{-5}	7.8×10^{-3}	1.2	5.6×10^{-3}
3	1024	335	2×10^{-5}	7.1×10^{-3}	1.4	5.3×10^{-3}
4	256	419	8×10^{-5}	1.1×10^{-3}	2.1	7.9×10^{-3}
4	512	457	1.5×10^{-5}	1.0×10^{-3}	3.0	5.6×10^{-3}
4	1024	335	4×10^{-6}	9.2×10^{-4}	3.8	5.5×10^{-3}

stationary state. This is done by adding a dissipation term $-\gamma\omega$, with $\gamma\approx0.01$, to the right-hand side of Eq. (1), restricted to large scales $0<|k|\leqslant3$. The number of involved modes allows rather isotropic large-scale dissipation and forcing.

A mild spectral filter has been used, without complete dealiasing. Dealiasing conserves energy and enstrophy [20,8], but not other inviscid constants of motion. Hence, it could artificially favor a power-law behavior based on these quantities [21].

The use of normal viscosity requires more computational resources than hyperviscosity. The real Navier-Stokes equation has normal viscosity, and hyperviscosity is known to affect some of the statistical properties. To avoid this degree of uncertainty normal viscosity is used in the simulations here.

The slope of the energy spectrum equilibrates quickly and fluctuates little with time. Long runs showed no drift in the energy spectrum. Table I lists the runs together with several of their parameters. The first column defines the type of flow by a parameter α introduced later in the text. The Navier-Stokes equation corresponds to $\alpha=2$.

B. Inertial range spectrum

The enstrophy spectrum $H(k)=\int_{|\vec{k}|=k}|\hat{\omega}|^2 d\vec{k}$, is shown in Fig. 1 for various Reynolds numbers. The slope in the inertial range becomes flatter as the Reynolds number increases.

The spectra are averaged over several instants of time. While the spectra hardly change with time, averaging over several snapshots smooths the wiggled spectra and aids in this way the determination of slopes. Local slopes can be extracted using one of the usual methods of numerical differentiation. Rather similar slopes are obtained from fitting a straight line to the spectrum on a log-log plot (points with error bars in Fig. 2). The error bars result from fitting different ranges and also comparing with local slopes.

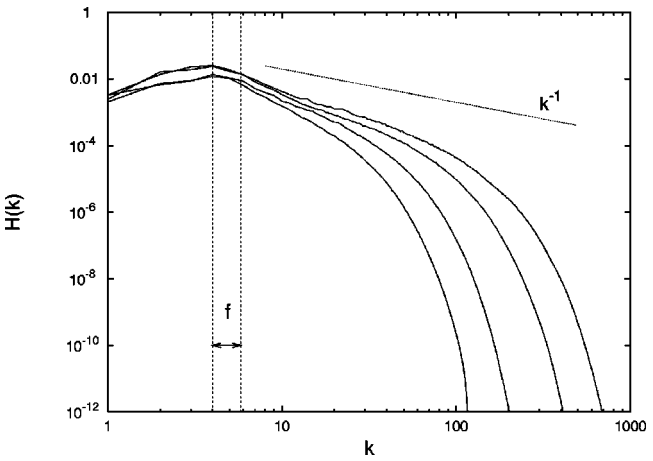

FIG. 1. Enstrophy spectra for the Navier-Stokes equation for different Reynolds numbers. Forcing acts on large scales. The dotted line has slope -1. There is a visible change of the inertial range slope with Reynolds number.

A logarithmically corrected power law is also fitted to the inertial range $Ck^{-1}(k/k_d)^{s+1}\log(k/k_I)^{-(3+s)/(7+s)}$. This particular form follows Ref. [10] and reduces to the closure prediction for $s=-1$. The wave number k_I is the forcing scale, $k_I\approx5$, k_d the dissipation scale, and C is a constant. The fitted s is insensitive to the choice of k_d. For the purpose of comparison, the Reynolds number R_L used in Fig. 2 is defined in the same way as in Ref. [10]

$$R_L=\frac{UL}{D},\quad U=\sqrt{\langle v^2\rangle},\quad L=\frac{1}{2}\frac{U}{\langle D(\nabla\omega)^2\rangle^{1/3}}. \qquad (2)$$

U and L are a velocity and length scale respectively. The parameter s is shown in Fig. 2 as diamonds. The measurements agree within errors with simulations by Gotoh [10] at resolutions ranging up to 4096×4096. They are shown in Fig. 2 as discs, to be compared with the diamond symbols.

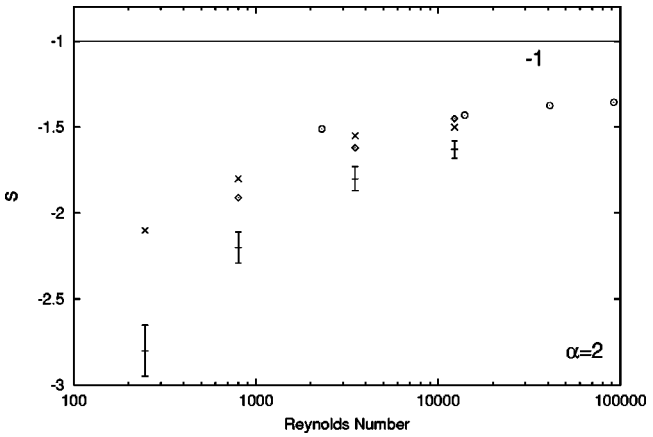

FIG. 2. Slope of the enstrophy spectrum of the two-dimensional Navier-Stokes equation versus Reynolds number R_L. The different types of points correspond to a simple power law k^s (error bars), a logarithmically corrected power law of the form $k^{-1}(k/k_d)^{s+1}\log(k/k_I)^{-(3+s)/(7+s)}$ ($\diamond$), the same from simulations by Gotoh ($\odot$), and the slope of the background field ($\times$). The slope of the energy spectrum is the slope of the enstrophy spectrum minus 2.

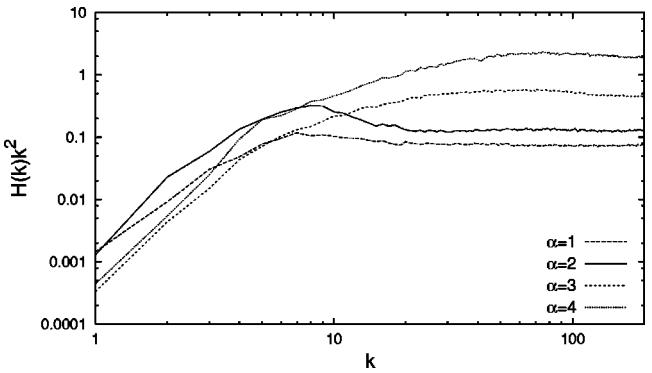

FIG. 3. Spectra of enstrophy concentrations ($|\theta|>2\theta_{\rm rms}$) in the large-scale and inertial range.

Whatever the assumed functional form and the procedure to determine the slopes, a clear flattening with Reynolds number is evident. The energy spectrum is simply related to the enstrophy spectrum by $E(k)=H(k)/k^2$. From Fig. 2 one can rule out $E(k)\sim k^{-4}$, but not $k^{-11/3}$. It is most plausible that k^{-3} (with perhaps logarithmic corrections) is asymptotically reached.

The steeper slope measured in many earlier simulations might simply be explained by the low resolution (and therefore low Reynolds number). There are several venues of explanation. Flow at low Reynolds number could really have a steeper spectrum. Coherent structures and intermittency effects have been proposed to this end. Another possible explanation is that ''local'' interactions among wave vectors are still spread over a substantial range of wave numbers, comparable to the size of the inertial range in numerical simulations. Or the higher slopes might have been due to numerical artifacts, e.g., an insufficient number of represented modes or insufficient integration time.

C. Decomposition into strong vortices and background field

A few, large coherent structures can dominate the energy spectrum over a substantial range of wave numbers. If the vortices are distributed by themselves with ever and ever smaller length scale, they can also determine the form of the spectrum over the entire inertial range. Decomposition into coherent structures and background flow has been applied to decaying turbulence [18,19] and to turbulence forced at small scales [9]. Here we shall apply the same decomposition to turbulence with forcing at large scales.

The procedure [18,19,9] decomposes the domain into a small region of high enstrophy and a large remaining region of background flow. The cutoff level is chosen at $2\omega_{\rm rms}$. The slopes depend on the cutoff level for ω, but only weakly at this value for the cutoff. The background flow covers 94–97 % of the domain, in agreement with an approximately Gaussian distribution for ω [12,22]. Applying this procedure, the slopes of the background flow are shown in Fig. 2 as crosses. The background field has systematically a flatter slope, but with the same asymptotic behavior as the complete flow.

The foreground field (the strong vortices) has a clear k^{-2} spectrum, as shown in Fig. 3 (solid line). This behavior is independent of the Reynolds number.

III. α TURBULENCE

A. Introduction

In this section we investigate other two-dimensional flows. A particular family of flows, collectively called ''α turbulence,'' has recently attracted attention as model equations for the study of turbulence and singularities (see, e.g., Refs. [23–26,22]).

The flows are described by advection-diffusion equations

$$\frac{\partial\theta}{\partial t}+\vec{v}\cdot\vec{\nabla}\theta=D\vec{\nabla}^2\theta+f. \tag{3a}$$

The scalar quantity advected is $\theta(\vec{r},t)$. The velocity $\vec{v}(\vec{r},t)$ is a function of θ, best written in Fourier space,

$$\hat{\vec{v}}(\vec{k},t)=i\frac{\vec{k}^{\perp}}{k^{\alpha}}\hat{\theta}(\vec{k},t). \tag{3b}$$

We write k for $|\vec{k}|$. The symbol $\vec{k}^{\perp}$ indicates a vector of length $|\vec{k}|$ and direction perpendicular to $\vec{k}$. It follows that $\nabla\cdot\vec{v}=0$. The forcing is again white-in-time.

Different values of α correspond to different flows [25]. The two-dimensional Navier-Stokes equation (1) is recovered for $\alpha=2$ and θ corresponds to ω. The surface quasigeostrophic equation, $\alpha=1$, is a special case of quasigeostrophic flow, as relevant for planetary atmospheres and oceans [23]. In this case, θ is physically interpreted as temperature, which determines the velocity field through its buoyancy effect. A third equation considered is $\alpha=3$ which arises in geophysical context as a shallow flow on a rotating sphere with uniform internal heating [27].

One can study Eq. (3) also for values of α not physically realized. It can be considered as a model system parametrized by α, which, in view of Eq. (3b), controls the dependence of v on θ. Only the nonlinear term $\vec{v}\cdot\nabla\theta$ in Eq. (3a) couples different modes and generates small-scale turbulence from the large-scale forcing. In Fourier space Eq. (3) translates into

$$(\partial_t+Dk^2)\,\hat{\theta}(\vec{k},t)=\int d\vec{k}'\frac{i\vec{k}\cdot\vec{k}'^{\perp}}{\vec{k}'^{\alpha}}\hat{\theta}^*(\vec{k}')\,\hat{\theta}(\vec{k}-\vec{k}')+\hat{f}(\vec{k},t).$$

Here, the influence of α on the coupling between modes is seen explicitly.

Borrowing terminology from the Navier-Stokes equation, the conserved quantity $\frac{1}{2}\theta^2$ shall be called ''enstrophy.'' As a consequence of Eq. (3a) enstrophy moves from the forcing to the dissipation scale. The left hand side of Eq. (3a) conserves $\langle\theta^n\rangle$ for all α and positive integers n. Another conserved quadratic quantity is $\psi\theta$, which however does not need to be positive and it is not local. Here the stream function ψ is given by $\hat{\psi}(\vec{k},t)=\hat{\theta}(\vec{k},t)/k^{\alpha}$. The kinetic energy $\frac{1}{2}\langle\vec{v}^2\rangle$ is only conserved for certain values of α, when it coincides with either $\langle\theta^2\rangle$ or $\langle\psi\theta\rangle$.

Equation (3) is invariant under $\vec{r}\to\vec{r}\lambda$, $t\to t\lambda^2$. This invariance naturally defines a Reynolds number for flow of any α as ${\rm Re}=UL/D$. We choose $U=\sqrt{\langle\vec{v}^2\rangle}$ and $L=1$ for a

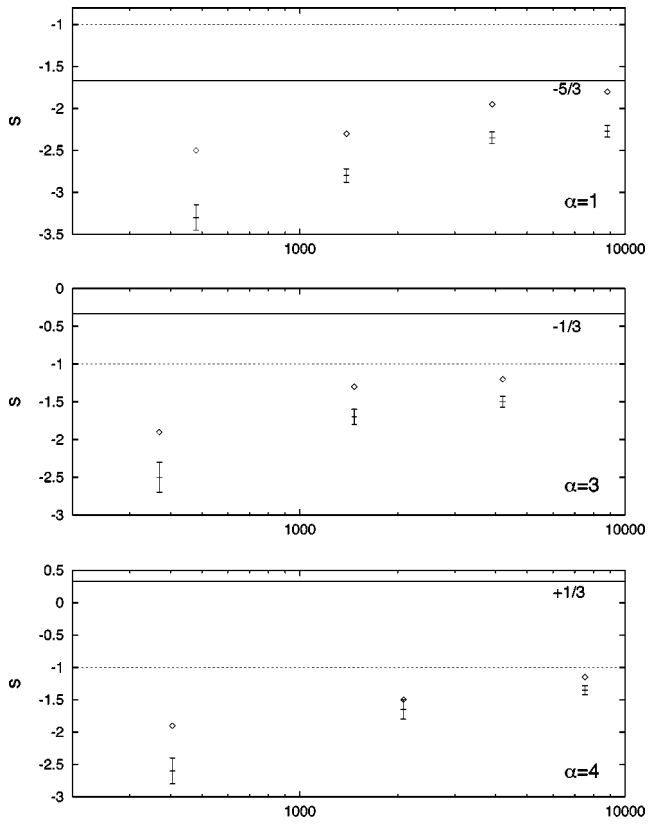

FIG. 4. Slope of the enstrophy spectrum for flows with $\alpha = 1,3,4$ as a function of Reynolds number Re. Points with error bars correspond to the complete flow; crosses to the background flow. Solid and dashed lines are theoretical values for asymptotically large Reynolds number.

large-scale Reynolds number Re. With this definition the Reynolds number Re takes on only slightly different values from R_L used before (2).

B. Results

The flows for different α are simulated and analyzed in the same way as described in Sec. II for the Navier-Stokes equation. The scalar θ takes on the role of ω. The slopes for a simple power law are shown in Fig. 4. Since, from Eq. (3b), $|\hat{\vec{v}}(\vec{k})|^2 = |\hat{\theta}(\vec{k})|^2 / k^{2(\alpha-1)}$, the slopes of the energy and enstrophy spectrum differ precisely by $2(\alpha-1)$. In each part of Fig. 4 a clear dependence on Reynolds number is seen. The background flow shows a systematically flatter slope.

Previous studies of the energy spectrum for flows with $\alpha \neq 2$ and $\alpha \neq 1$ are due to Pierrehumbert *et al*. They use hyperviscosity to extend the inertial range and hence observe flatter slopes, even at lower resolution.

Figure 5 provides an overview of slopes as a function of α. Shown are the slopes for the complete flow fields (triangles), the background fields (crosses), and data by Pierrehumbert *et al.* (circles) [24]. The slopes displayed are for the highest Reynolds number measured and are hence steeper than for asymptotically high Reynolds number. Finite-time singularities for $\alpha < 1$ pose questions on the validity of the numerical scheme.

Values of $\alpha = 1$ and 2 are both special, since they conserve kinetic energy. A run for $\alpha = 1.5$ at a resolution of

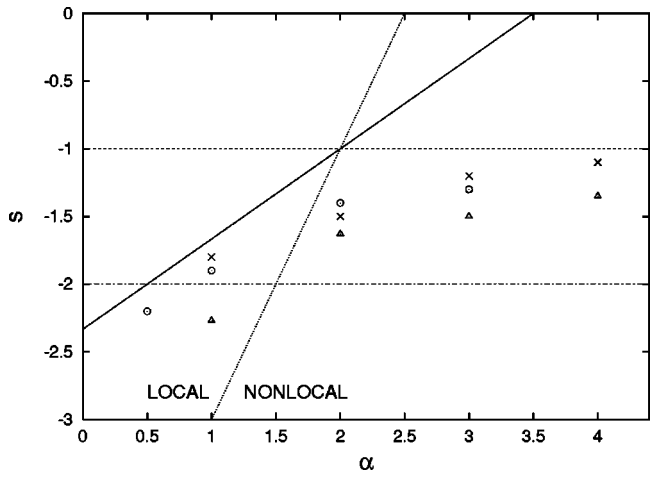

FIG. 5. Slopes of the enstrophy spectrum versus α (ignoring possible modifications to a pure power law). Shown are the slopes at the highest Reynolds number ($\triangle$), the slopes of their background field ($\times$), and data by Pierrehumbert *et al.* ($\odot$) who used hyperviscosity. At higher Reynolds numbers the spectra become flatter. The solid, dashed, and dash-dotted line are theories for asymptotically large Reynolds number. The dotted line roughly separates local and nonlocal enstrophy transfer, based on a dimensional estimate.

512×512 produced intermediate values between $\alpha = 1$ and 2 at the same resolution, so that there is no discernible qualitative difference.

Also the decomposition into background and foreground field is carried out as before. Figure 3 shows the enstrophy spectra of the foreground at a resolution of 1024×1024, i.e., comparable Reynolds number. A different behavior is seen for $\alpha \leqslant 2$ and $\alpha > 2$. In the first case, regions of large enstrophy are roundish (elliptical), while in the later they form filaments (Fig. 6). As discussed below, this conforms with the idea that the small scales are dominated by large-scale shear only for $\alpha > 2$.

C. Comparison with theory

Pierrehumbert *et al.* [24] suggested the spectra of α turbulence could be explained by a local enstrophy cascade in one region of α and a Batchelor-type passive scalar behavior in another. Indeed this finds strong support from the data.

Classical dimensional analysis states that only k and the enstrophy dissipation are physically important. From the dimension of velocity $[v] = L/T$, the dimension of the scalar $[\theta] = L^{2-\alpha}/T$ follows using Eq. (3b). One arrives at the prediction of an ''enstrophy cascade'' [24]

$$H(k) \sim (d\langle \theta^2 \rangle / dt)^{2/3} k^{-7/3+(2/3)\alpha}. \tag{4}$$

These predictions are drawn as solid lines in Figs. 2, 4, and 5. They agree with the data for $\alpha \leqslant 2$. For $\alpha > 2$ the slopes do not seem to approach the enstrophy prediction and never become flatter than -1.

The cascade argument requires a sufficiently local enstrophy transfer [2]. The criterion is the mean-square shear, which behaves as $\int k^2 E(k) dk$ [2]. The spectrum $E(k)$ is based on the velocity, $E(k) = \int_{|\vec{k}|=k} |\hat{\vec{v}}|^2 d\vec{k}$. This limits the

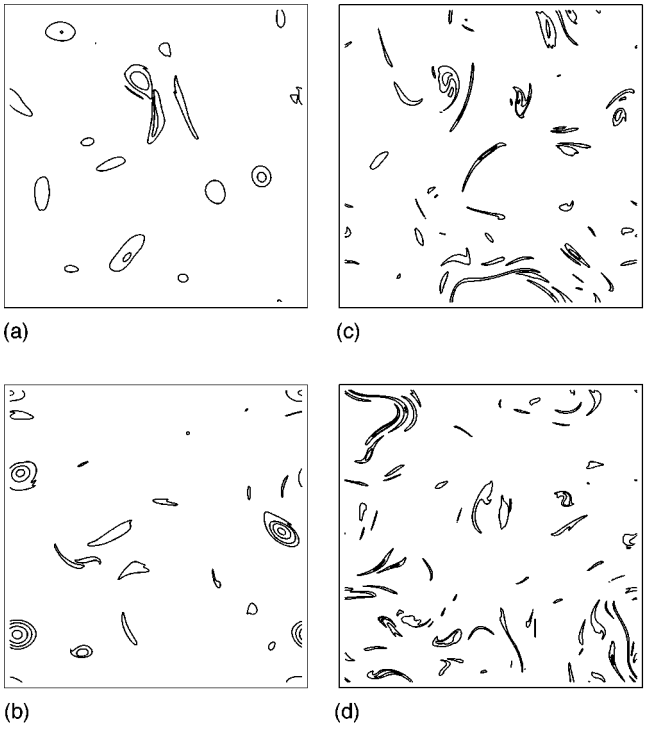

FIG. 6. Contour plot of the scalar θ in regions of large enstrophy $\theta^2 > 4\langle\theta^2\rangle$ for (a) $\alpha=1$, (b) $\alpha=2$, (c) $\alpha=3$, and (d) $\alpha=4$. In (a) and (b) elliptic structures predominate, while (c) and (d) show many thin filaments. Contour lines are drawn at $\pm 2\theta_{\rm rms}$, $\pm 3\theta_{\rm rms}$, $\pm 4\theta_{\rm rms}$, and so on.

validity of Eq. (4) to $\alpha<2$. For $\alpha>2$ the transfer is not expected to be spectrally local. Figure 5 shows the separation of local and nonlocal transfer based on above integral estimate (leading to $s=2\alpha-5$) as a dotted line.

Another important transition takes place also at $\alpha=2$. The typical time scale of motion as a function of wave number changes. Based on either Eq. (4) or (5), the fast motion shifts from small scales to large scales. For $\alpha>2$ the small scales do not have enough time to equilibrate, before they are moved around by the large scale motion over substantial distances. There is no time to reach ''Kolmogorov equilibrium.''

This leads to the idea that a passive scalar spectrum might be applicable. The classical theory of the passive scalar spectrum in two-dimensional turbulence [28] leads indeed to a k^{-1} spectrum and has also been suggested as an alternative explanation of the Navier-Stokes enstrophy spectrum [5]. Batchelor's [28] derivation does not make use of the functional dependence of the velocity, since it is for a passive scalar. Hence the k^{-1} form generalizes to any α, and can be justified for $\alpha\geqslant 2$ because of the aforementioned nature of time scales. To reproduce this spectrum by dimensional analysis one assumes k and the absolute size of the enstrophy $\langle\theta^2\rangle$ are physically important. One obtains

$$H(k)\sim\langle\theta^2\rangle k^{-1} \tag{5}$$

independent of α. The dashed lines in Figs. 4 and 5 are drawn at an exponent of -1. Apparently no enstrophy spectrum for our α-turbulence is flatter than k^{-1}.

The data agree with Eq. (4) for $\alpha<2$ and Eq. (5) for $\alpha>2$. The validity of either approach is theoretically particularly questionable for $\alpha=2$, yet both coincide and appear to be correct (besides logarithmic corrections). Exactly at this crossover lies the Navier-Stokes equation. Here both Eqs. (4) and (5) are dimensionally correct, because θ contains only units of time. Only here coincides the theory of enstrophy cascades with passive advection of small scales.

The idea that (well-separated) step discontinuities in the enstrophy distribution determine the spectrum [15] leads to $H(k)\sim k^{-2}$ for all α and is ruled out by the data (see dash-dotted line in Fig. 5). Incidentally, the strong enstrophy concentrations considered in isolation form precisely a k^{-2} spectrum for $\alpha=1$ and $\alpha=2$, as seen in Fig. 3. The qualitative difference in the foreground field for $\alpha\leqslant 2$ and $\alpha>2$ is also clearly seen in Fig. 6. By definition, the foreground flow field is set to zero where $|\theta|<2\theta_{\rm rms}$. Saffman's argument explains the k^{-2} behavior in this case: as a consequence of the decomposition procedure, a one-dimensional cut through the field shows (well-separated) step discontinuities. Why the foreground spectrum for $\alpha=2$ is more similar to that of $\alpha=1$ than to $\alpha=3$ is unclear.

For the background field we note from Figs. 2 and 4 that the difference in slope between the complete field and the background field is reduced with increased Reynolds number. The last data point for $\alpha=1$ appears as exception. In total, there is no evidence for any discrepancy in the two slopes for asymptotically high Reynolds number.

IV. GENERAL THEORY

The conclusions are drawn and discussed in the context with various other results (e.g., Refs. [28,2,13,9,24,29,10]) on two-dimensional turbulence.

Steepening by large structures. Concentrations of large enstrophy (''strong vortices'') lead to a steepening of the spectrum for any kind of α turbulence. However, they have less influence on the spectrum at higher Reynolds number. For the two-dimensional Navier-Stokes equation this was already suggested by earlier observations [13]. Asymptotically the flow field appears to approach the same inertial range spectrum with or without its large vortices taken into account. For the Navier-Stokes equation without forcing or with small-scale forcing, coherent vortex structures have also been observed to steepen the spectrum, may it be over a limited range of wave numbers or for the entire inertial range. For large-scale white-in-time forcing an *asymptotic* steepening is *not* supported by the data.

Enstrophy dissipation based scaling. For the Navier-Stokes equation the enstrophy dissipation based scaling law is in good agreement with numerical simulations, even when normal (genuine) viscosity is used. The energy spectrum flattens with Reynolds number and appears to approach k^{-3} (k^{-1} for the enstrophy), with logarithmic corrections to this power law certainly possible [10,13]. The same theory as for the Navier-Stokes equation applies to other flows as long as the enstrophy transfer may be assumed to be dominated by local strain (''local enstrophy cascade''). In this case, dimensional analysis based on enstrophy dissipation correctly describes the inertial range energy spectrum within a power law approximation.

Passive scalar based scaling. The cascade argument loses its self-consistency for the two-dimensional Navier-Stokes equation, since it predicts in this case a marginally nonlocal transfer. For nonlocal enstrophy transfer one expects passive advection of the scalar by strain fields varying slowly in space. The enstrophy spectrum is steeper than would be expected on the basis of local transfer. In this sense one can say that nonlocality steepens the spectrum. The data support an asymptotic k^{-1} form in agreement with passive scalar behavior.

ACKNOWLEDGMENTS

I am grateful to Alexander Bershadskii, Jeff Chasnov, Emily Ching, Alexandre Chorin, Toshiyuki Gotoh, and Raymond Pierrehumbert for valuable communications. This work was supported by the Chinese University of Hong Kong and by the Research Grants Council of the Hong Kong Special Administrative Region, China (RGC Ref. No. CUHK4119/98P).

[1] G. Batchelor, Phys. Fluids Suppl. II **12**, 233 (1969).
[2] R. Kraichnan, Phys. Fluids **10**, 1417 (1967).
[3] C. Leith, Phys. Fluids **11**, 671 (1968).
[4] U. Frisch, *Turbulence* (Cambridge University Press, Cambridge, 1995).
[5] R. Kraichnan and D. Montgomery, Rep. Prog. Phys. **43**, 547 (1980).
[6] M. Lesieur, *Turbulence in Fluids*, 3rd ed. (Kluwer Academic Publishers, Dordrecht, 1997).
[7] K. Nakamura, T. Takahashi, and T. Nakano, J. Phys. Soc. Jpn. **62**, 1193 (1993).
[8] J. R. Chasnov, Phys. Fluids **9**, 171 (1997).
[9] V. Borue, Phys. Rev. Lett. **72**, 1475 (1994).
[10] T. Gotoh, Phys. Rev. E **57**, 2984 (1998).
[11] Y. Hibino and T. Gotoh, Proc. Res. Inst. Math. Sci. (Kyoto Univ.) **921**, 110 (1995).
[12] H. Takahashi and T. Gotoh, Proc. Res. Inst. Math. Sci. (Kyoto Univ.) **972**, 163 (1996).
[13] V. Borue, Phys. Rev. Lett. **71**, 3967 (1993).
[14] P. Tabeling, Phys. World **11**, 23 (1998).
[15] P. Saffman, Stud. Appl. Math. **50**, 377 (1971).
[16] A. Gilbert, J. Fluid Mech. **193**, 475 (1988).
[17] H. Moffatt, in *Advances in Turbulence*, edited by G. Comte-Bellot and J. Mathieu (Springer-Verlag, Berlin, New York, 1986), p. 228.
[18] R. Benzi, S. Patarnello, and P. Santangelo, Europhys. Lett. **3**, 811 (1987).
[19] R. Benzi, S. Patarnello, and P. Santangelo, J. Phys. A **21**, 1221 (1988).
[20] C. Canuto, M. Y. Hussaini, A. Quarteroni, and T. A. Zang, *Spectral Methods in Fluid Dynamics* (Springer, New York, 1988).
[21] A. Chorin, *Vorticity and Turbulence* (Springer Verlag, New York, 1994).
[22] N. Schorghofer, Phys. Rev. E **61**, 6568 (2000).
[23] I. Held, R. T. Pierrehumbert, S. Garner, and K. Swanson, J. Fluid Mech. **282**, 1 (1995).
[24] R. T. Pierrehumbert, I. M. Held, and K. L. Swanson, Chaos, Solitons and Fractals **4**, 1111 (1994).
[25] P. Constantin, SIAM (Soc. Ind. Appl. Math.) Rev. **36**, 73 (1994).
[26] P. Constantin, A. Majda, and E. Tabak, Nonlinearity **7**, 1495 (1994); K. Ohkitani and M. Yamada, Phys. Fluids **9**, 876 (1997); D. Cordoba, Proc. Natl. Acad. Sci. USA **94**, 12 769 (1997); P. Constantin, Q. Nie, and N. Schorghofer, Phys. Lett. A **241**, 168 (1998); P. Constantin, Q. Nie, and N. Schorghofer, Phys. Rev. E **60**, 2858 (1999).
[27] S. Weinstein, P. Olson, and D. Yuen, Geophys. Astrophys. Fluid Dyn. **47**, 157 (1989).
[28] G. Batchelor, J. Fluid Mech. **5**, 113 (1959).
[29] K. Oetzel and G. Vallis, Phys. Fluids **9**, 2991 (1997).